ELSEVIER

Thermochimica Acta 363 (2000) 129–135

thermochimica acta

www.elsevier.com/locate/tca

Nanocrystalline and metastable phase formation in vacuum thermal decomposition of calcium carbonate

S. Dash, M. Kamruddin, P.K. Ajikumar, A.K. Tyagi, Baldev Raj*

Metallurgy and Materials Group, Indira Gandhi Centre for Atomic Research, Kalpakkam 603102, India

Received 27 April 2000; accepted 6 July 2000

Abstract

Well characterised, polycrystalline powders of commercially procured $CaCO_3$ were thermally decomposed in the vacuum as well as in the flowing gas atmosphere for the purpose of studying solid state transformations. The characterisation of the end product CaO, obtained from the thermal decomposition, revealed contrasting features in the powder X-ray diffractograms. While the flowing gas method, conducted inside a thermogravimetric analyser (TGA), indicated formation of stable microcrystalline calcia, the decomposition under dynamic vacuum revealed formation of metastable-nanocrystalline calcia. The latter study was carried out in an evolved gas analysis-mass spectrometry (EGA-MS) facility. Experiments were also conducted inside the high temperature XRD (HTXRD) machine. The paper attempts to bring out possible mechanisms responsible for formation of these end products with such glaring structural contrast. Non-equilibrium conditions prevalent under dynamic vacuum condition as well as misfit strain energy available from $CaCO_3$/CaO interface are presumed to be the reason behind such metastable transformations. Kinetic analysis of the transformation revealed prevalence of nucleation and growth phenomena. Corresponding Arrhenius factors were also calculated.

Keywords: Thermal decomposition; Diffractograms; Non-equilibrium; Metastable-nanocrystalline phase; Nucleation and growth

1. Introduction

The thermal decomposition of $CaCO_3$ has been studied for the past many 100 years and it is well established that experimental conditions influence the properties of the end product. Knowledge of the decomposition process and its accurate control are relied upon to achieve reproducible CaO. Early investigations on $CaCO_3$ were prompted in the context of the manufacture of Portland cement [1]. Over the centuries, $CaCO_3$ and CaO have found very wide applications. Probably, $CaCO_3$ is the largest quantity of any raw material used by the chemical industry; as a fluxing agent in steel industry, in the manufacture of mortars, plasters, refractories, glass, additives, etc. CaO is used as raw material in the manufacture of sodium carbonate, calcium carbide, calcium sulphite and as $Ca(OH)_2$ in many chemical industries.

In recent times, $CaCO_3$ fillers are added to polymers for improvement in thermal and mechanical properties of the latter [2]. $CaCO_3$ is also encountered as an intermediate compound in the thermal decomposition of oxalates [3] and formates [4]. Hassanein has examined the decomposition of TALC–$CaCO_3$ from the view point of complex silicate formation [5]. Das [6] and Gracia-clavel et al. [7] have studied $CaCO_3$ decomposition from the view point of ternary oxide formation. Felder-Casagrande et al. has studied

* Corresponding author. Tel.: +91-4114-88518; fax: +91-4114-40301/+91-4114-40360.
E-mail address: dmg@igcar.ernet.in (B. Raj).

0040-6031/00/$ – see front matter
PII: S0040-6031(00)00604-3

decomposition of limestone $(CaMgCO_3)_2$ from CO_2 emission mitigation angle [8]. Besides the above practical applications, Wang and Mc Enancy have used temperature programmed decomposition (TPD) runs of $CaCO_3$ as EGA-MS calibrant [9].

The phenomenology of thermal decomposition and effect of variation in physical parameters on the decomposition have also been investigated. Maciejewski and Osward conducted morphological observation regarding role of vacuum on decomposition and observed that the initiation temperature for decomposition is lower in vacuum [10]. In a contemporary paper, Maciejewski et al. studied the effect of gaseous product pressure on decomposition [11]. Romeo Salvador et al. [12] and Criado and Ortega [13] have studied influence of particle size on the process. Role of oxide surface semiconductivity in reducing activation energy has also been experimented [14]. Several workers have also studied kinetics of thermal decomposition. Price et al. [15] have studied the kinetics and evaluated activation energy for vacuum decomposition to be around 184–197 kJ/mol using mass spectrometer. Kinetic constants were also determined by Topar et al. [16]. Since the advent of thermal analysis, the single step decomposition of $CaCO_3$ has been the most frequently investigated process. More than a couple of hundred publications on the thermal decomposition of $CaCO_3$ under isothermal, non isothermal, in different inert gas atmospheres and vacuum conditions have virtually given it a status of model reactant.

In contrast, the work on phase transition relating to $CaCO_3$ decomposition has been rather sparse. Available studies pertain to aragonite to calcite (A→C) transformation [17]. DTA and DSC techniques have been used by Morales et al. [18]. Thermally weak crystallographic transition (A→C) has also been diagnosed by Dubrawski and England [19]. Epple has carried out temperature resolved XRD to identify various structures [20]. Most exciting aspect of calcite decomposition remains the state of final product. In vacuum thermal decomposition, a metastable form of calcia has been identified [21]. However, there has been very little or practically no investigation on the state of the crystalline final product calcia. XRD investigations on air decomposed calcite giving stable calcia phase exist in literature. But metastable phase formation encountered in vacuum thermal decomposition needs better assessment. Practically no insight has been obtained to unravel the origin of metastability and formation of nanocrystallinity. In the light of the above, the thermal decomposition of $CaCO_3$ was studied by us using evolved gas analysis-mass spectrometry (EGA-MS) and TGA. The crystallochemical characterisation of various phases by XRD and HTXRD was carried out in an attempt to give a possible explanation to the origin of metastable CaO and its nanocrystalline state.

2. Experimental

LR Grade $CaCO_3$ powder samples procured from M/s Fischer Inorganics & Aromatics Ltd., Chennai were used in this study. Powder particles collected through a 50 μm stainless steel mesh were used for the investigations. Examination by a polarised light optical microscope (OM) in the dark field reflection mode showed that the particle size distribution peaked around 40 μm. Trace metallic impurities in this compound were determined using an ELAN 250 inductively coupled plasma mass spectrometer (ICP-MS) from SCIEX, Canada. The instrument was calibrated using synthetic, spectroscopically pure NBS traceable standards. The samples were dissolved in spectroscopically pure reagents and sprayed to ICP by use of a peristaltic pump and a Meinhard nebulizer. Data were acquired by rapid scan mode. Concentration of metallic impurities found in μg/g level are presented in Table 1. The raw sample was also analysed by SIEMENS D 500 diffractometer.

The powder $CaCO_3$ (100 mg) sample was subjected to EGA-MS runs at 6 K/min heating rate in the temperature range 300–1200 K. The details of the experimental facility have been described elsewhere

Table 1
Concentration of metallic impurities in $CaCO_3$ as analysed by ICP-MS

Element	Concentration in μg/g	Element	Concentration in μg/g
Al	<10	Mn	10
Ba	<10	Mo	<10
Co	20	Pb	<10
Cu	<10	Sr	27.5
Cr	<10	Zn	30
V	<10		

[22,23] and only a brief description is given below. This facility consists of a high vacuum, high temperature programmable resistance furnace coupled to an ultra high vacuum (UHV, 10^{-10} mbar) all metal stainless steel chamber through a variable conductance molecular leak valve. The high vacuum chamber is pumped by a turbo molecular pumping unit (TMPU). The UHV chamber, housing the quadrupole mass spectrometer (QMS) and other metrological hardware like magnetron gauge, spinning rotor gauge (SRG) is pumped by a combined sputter ion-titanium sublimation pump (ISP). The ISP is backed by a separate TMPU. The UHV chamber is also fitted with calibration gas inlets. The sample is taken in a platinum crucible and inserted into the resistance furnace for programmed heating. Previously calibrated K-type thermocouples, kept in contact with the crucible are used to measure the specimen temperature and it is also acquired through a PC based add-on card. The ion intensities of various product gases and sample temperature were tracked by a locally developed PC based software, which executes the real time multiple ion detection (MID) mass spectrometry. The MID signals are plotted against absolute temperature of sample to yield the EGA-MS spectra on TPD.

The TGA/DTA runs of $CaCO_3$ were conducted in a SETARAM model SETSYS 16/18 thermogravimetric analyser under ultra high pure (UHP, 99.99%) helium carrier gas flow of 25 ml/min. The TGA runs were conducted at a heating rate of 6 K/min in the temperature range 300–1200 K. The experimental parameters for TGA run were kept similar to EGA-MS run to enable suitable comparison. Prior to acquisition of the thermograms, the system was temperature calibrated by recording the endothermic melting transitions of UHP metals like In, Pb, Al, Au and Pd. The thermograms were corrected for buoyancy and background.

3. EGA-MS and TGA studies

Calcium carbonate undergoes single step decomposition process under vacuum according to the expression $CaCO_3^s(s) \rightarrow CaO^s + CO_2^g(g)$, where s and g refer to solid and gas, respectively. The decomposition process was studied both by EGA-MS and TGA runs. Profiles are shown in Fig. 1(a). During

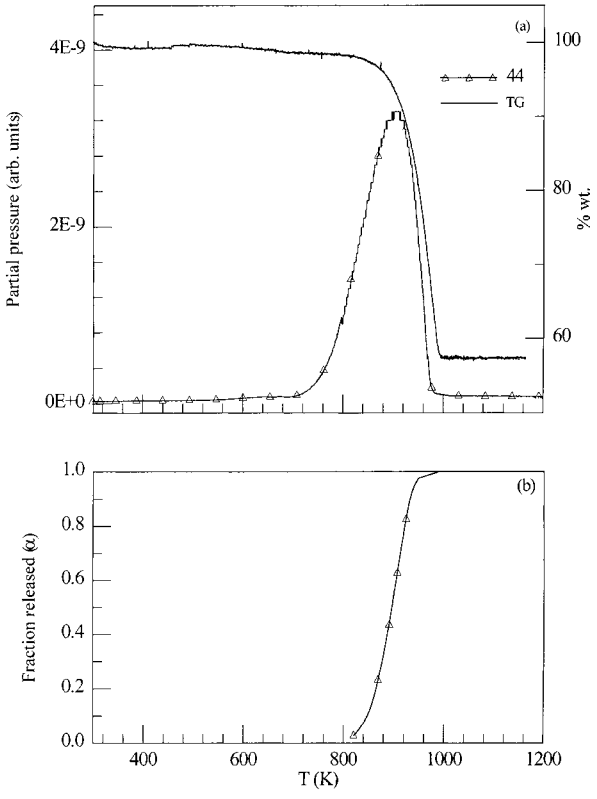

Fig. 1. (a) EGA-MS Spectra of TPD of $CaCO_3$ at 6 K/min heating rate with the TGA Plot is superimposed on it; (b) the fraction release plot for CO_2 obtained from EGA-MS spectra.

these runs, the QMS was tuned to $m/e = 44$ and $m/e = 28$ pertaining to decomposition product CO_2 and its electron impact generated fragment CO, respectively. The single step decomposition spanned over a temperature range 700–1000 K and has a maximum release rate at 890 K. The CO/CO_2 ratios approximately matched the CO_2 fragmentation intensity ratio provided by QMS. For explaining weight loss, TGA curve was superimposed over EGA-MS spectra. TGA weight loss depicts a higher onset temperature (800 K) for the decomposition compared to EGA. The inflexion in TGA curve occurs at 940 K. The decomposition in TGA occurs over a narrower temperature width. The higher onset and inflexion temperature in TGA can be due to lower superficial velocity of He carrier gas as compared with dynamic high vacuum used in EGA, this can lead to slower removal of CO_2 product gas resulting in higher temperatures for reactions [24]. The narrower temperature

span observed in TGA for decomposition can be attributed to superior sample temperature uniformity ensured by convection of thermally conductive helium carrier gas [25]. The TGA weight loss of 44% is explainable solely on the basis of CO_2 emission.

4. Kinetic analysis

Fraction release plots of $CaCO_3$ decomposition obtained from EGA-MS data are shown in Fig. 1(b). The $\alpha_{(T)} \sim T$ curve is sigmoidal in character. The $\ln\{g(\alpha)/T^2\} \sim 1/T$ plots a correlation with random nucleation mechanism based on Mampel unimolecular law. The activation energy was evaluated to be 211 kJ/mol. The corresponding pre-exponential factor is 4.3×10^{11} s^{-1}. The activation energy value matches well with the value reported in the compilation by Maciejewski and Reller [26]. The random nucleation resulting from surface dominated phenomena of desorption of CO_2 gas emerges as controlling mechanism. High dislocation density [27] resulting in strained interface between rhombohedral calcite and cubic calcia favour the nucleation and growth by way of bringing down the activation barrier. Even though there is a product barrier formation leading to clear establishment of an intercrystalline interface, the expected diffusion control mechanism is not prevalent, perhaps due to porous nature of product layer yielding fast diffusion path. Pores and channels manifest due to interfacial mismatch between various crystallites [28].

5. XRD studies

Calcium carbonate ($CaCO_3$) occurring in nature contains three polymorphs, i.e. calcite (C), aragonite (A) and vaterite (V). The finely powdered material used in our investigations was examined by XRD. The plots are shown in Fig. 2(a). It contained aragonite and calcite with a proportion 3:2. Signature of the vaterite phase was not observed. Aragonite is a high pressure phase of calcite having orthorhombic structure with Pmcn space group. Calcite possesses rhombohedral cell having $R\bar{3}c$ space group [29]. It has two formula molecular units of $CaCO_3$ per unit cell [30]. The covalently bonded CO_3^{2-} oxyanion forming a planar

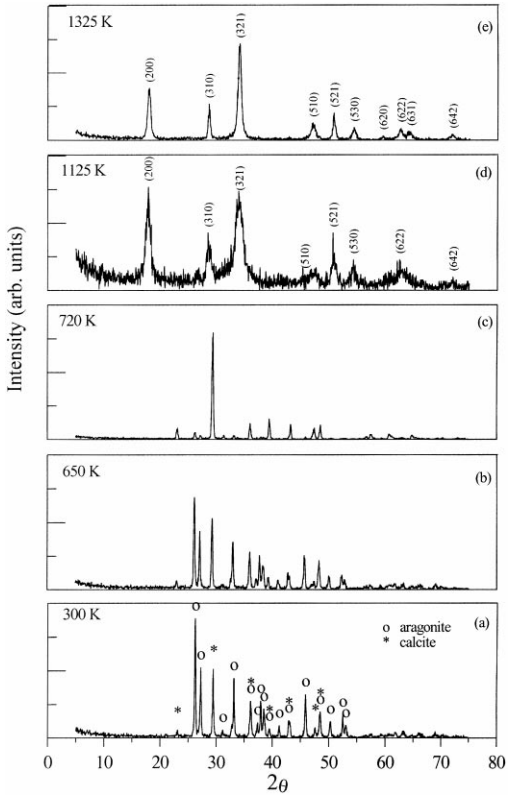

Fig. 2. Powder XRD patters of (a) aragonite dominated starting material; (b) calcite dominated material; (c) complete conversion to calcite; (d) nanocrystalline $Ca(OH)_2$; (e) thermal growth towards microcrystalline $Ca(OH)_2$.

equivalent triangle with carbon at the centre lies in a plane at right angle to the three-fold axis. Each consecutive group is orientationally twisted. The calcium atoms occupy corners and the face centres of the cell and are hexa co-ordinated with six oxygen atoms of six different CO_3^{2-} groups. The oxygen is tri co-ordinated. In contrast, aragonite is densely packed. The Ca atom is nine co-ordinated with oxygen and oxygen is tetra co-ordinated. This crystal chemical picture has direct bearing on thermal analysis. As the temperature was increased to 650 K, the aragonite fraction declined and at 720 K, complete conversion to calcite was observed (Fig. 2(b) and (c)). Though A→C transition could not be captured with TG/DTA, phase analysis of the sample at 650 and 720 K clearly revealed it. This transition is clearly in tune with the fact that higher temperature structures are more open and symmetric, favoured by entropy [31,32].

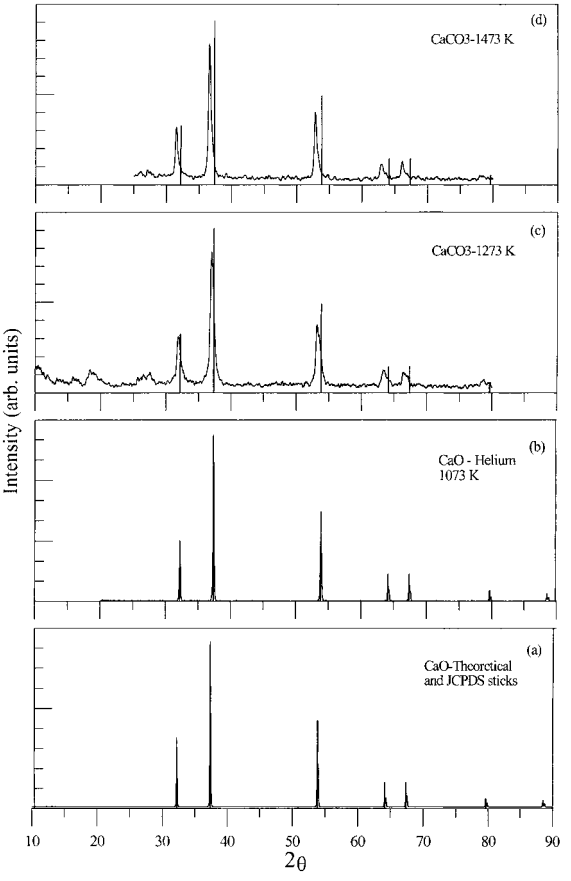

Fig. 3. (a) Theoretically generated, reference diffractogram of CaO; (b) diffractogram of calcia formed in a helium gas atmosphere; (c) HTXRD spectrum of calcia at 1273 K; (d) HTXRD spectrum of calcia at 1473 K.

Calcite to CaO conversion, though occurs before 1000 K, the XRD analysis revealed formation of a nanocrystalline $Ca(OH)_2$ hexagonal phase (Fig. 2(d)) at 1120 K. This phase persisted at 1320 K (Fig. 2(e)). The $Ca(OH)_2$ formation is due to instantaneous hydration of decomposition product calcia and it clearly indicated formation of extraordinarily reactive high surface area calcia crystallites as a precursor. As all our attempts to isolate and characterise the product failed, high temperature XRD (HTXRD) of $CaCO_3$ under 10^{-5} mbar vacuum was resorted to get the diffraction patterns. The patterns are depicted in Fig. 3(c) and (d). Both the patterns were found to be nanocrystalline and did not match with the JCPDS–ICDD sticks for CaO (Card No. 37–1497). A systematic angular shift was observed in the patterns obtained by us in vacuum. An examination of literature revealed that stable calcia phase is normally synthesised under flowing nitrogen dry gas [33]. This procedure was adopted and after heating $CaCO_3$ for more than 24 h under flowing dry helium, the sample was insulated from air with collodium amile acetate mixture in hot condition. XRD pattern acquired subsequently is shown in Fig. 3(b). The pattern was found to be microcrystalline and matched with stable calcia phase. To obtain the reference spectrum according to JCPDS–ICDD stick locations for stable calcia, the XRD pattern was theoretically generated by us through the use of the atomic form factors, lattice parameter and atom locations [34]. This pattern was used as a reference pattern and is shown in Fig. 3(a).

The patterns observed at 1273 and 1473 K were indexed to a cubic phase with a trial and error programme. The lattice parameters were found to be 0.485595 and 0.4883475 nm, respectively. A figure of merit better than 40 indicated reliable nature of the computations. The stable calcia has a lattice parameter of 0.481059 nm. This increment could possibly be due to anharmonic lattice dilatation leading to thermal expansion at high temperatures [35]. Considering Einstein model for the solid [36] and the expansivity reported by Ruppin [37], thermally induced dilatation was evaluated. However, the observed dilatation was much beyond thermal expansion regime. Hence, the excess increments 0.9 and 1.51% at 1273 and 1473 K can be ascribed to non-equilibrium metastable phase formation.

Concept of a metastable phase formation at the interface between decomposing rhombohedral calcite and cubic calcia product has been reported by Beruto and Searcy [38]. In a subsequent publication [21], the authors ruled out structural dissimilarity between metastable calcia and stable calcia. Only the volume expansion of metastable form was propounded. In a noteworthy investigation, Towe [39] used hot stage TEM to study calcite single crystal decomposition. The selected area diffraction (SAD) pattern revealed identical symmetry. CaO exhibited several topotactic transformations. Metastability of calcia was ascribed to the formation of small crystallites having size $\sim$10 nm.

In the light of the above, the particle size analysis of in-situ decomposed calcite was calculated by us from

X-ray line profile broadening analysis using Scherrer formula. The strongest line (200) was used for this. The full width at half maximum (FWHM) was evaluated after obtaining a Lorentzian fit. Machine contribution to line broadening was corrected. The crystallite sizes were found to be around 17 and 47 nm at 1273 and 1473 K, respectively. The enhanced crystallite size at 1473 can be ascribed to the thermal growth.

It is felt necessary to explain origin of nanocrystallinity as well as metastability of CaO generated under vacuum environment, which contrasts with stable CaO product observed in air and flowing gas decomposition. Obviously the dichotomy can be attributed to higher degree of non-equilibrium associated with vacuum thermal decomposition. In arial and flowing gas decompositions, the residence time of evolved gas is fairly larger in the decomposition chamber and hence prevalence of local equilibrium/quasiequilibrium conditions can not be ruled out. However, experiments conducted under dynamic high vacuum with high throughput turbomolecular pumps ensure perfect non-equilibrium condition for decomposition experiment to proceed.

At a microscopic level, the origin of metastability and nanocrystallinity can be attributed to non-equilibrium defects like dislocation substructure present in the material. Thomas and Renshaw had concluded that decomposition reactions in deformed calcite crystals are initiated only on dislocations gliding on certain planes [40]. This interface misfit strain energy can also be traced to atomic disregistry between rhombic $CaCO_3$ and cubic CaO. Considerable strain energy stored in dislocations not only promotes faster nucleation but is also responsible for extra-ordinary reactivity of the specimen. The nanocrystalline phase of materials has been attributed as a non-equilibrium state [41]. Sudden release of strain energy, energetically favour this metastable phase formation [42]. This is analogous to displacive microstructural transformations occurring in alloys [43]. Many newer techniques focusing on preparation of nanophase materials rely on physical means to prevent these phases from agglomerating to microcrystalline state. These methods exploit harsher non-equilibrium situations like high speed ball milling [44] and hydrodynamic cavitation [45]. In this case, it is prudent to expect this nanophase formation to be driven by elastic strain energy stored in dislocation network. Detailed in-situ investigations using TEM is being pursued to confirm the proposed hypothesis.

6. Conclusion

The contrasting features with respect to formation of end product of decomposition were revealed by XRD analysis. The vacuum decomposed calcite always yielded a metastable-nanocrystalline calcia where as flowing gas/air decomposed calcite yielded microcrystalline calcia. The sample environments have a clear bearing on the state of the final product. Non-equilibrium conditions prevalent in vacuum conditions are clearly responsible for the formation of nanocrystalline calcia, where as low gas flow rates causing local equilibrium conditions driven by accumulation of partial pressure of CO_2 results in formation of stable microcrystalline phase. Under dynamic high vacuum conditions, accumulation of p_{co_2} can be completely ruled out and the non-equilibrium nature of the process is fully ensured. It is proposed that the strain energy available from misfit dislocations caused due to atomic disregistry of $CaCO_3$/CaO interface, allows the system to be moved and get trapped in local minima rather than reaching a global minimum essential for stable phases.

References

[1] C. Guler, D. Dollimore, G.R. Heal, Thermochim. Acta 54 (1982) 187.
[2] B. Zerjal, V. Musil, B. Pregrad, T. Malovasic, Thermochim. Acta 134 (1988) 139.
[3] K.N. Ninan, C.G.R. Nair, Thermochim. Acta 30 (1979) 25.
[4] K.O. Hartman, I.C. Hisatsune, J. Phys. Chem. 69 (1965) 583.
[5] M. Hassanein, Thermochim. Acta 127 (1988) 171.
[6] C. Das, Thermochim. Acta 144 (1989) 363.
[7] M.E. Gracia Clavel, M.J. Martinez-Lopeard, M.T. Casais-alvarez, Thermochim. Acta 57 (1982) 223.
[8] S. Felder-Casagrande, H.G. Wideman, A. Reller, J. Thermal. Anal. 49 (1997) 971.
[9] J. Wang, B. Mc Enancy, Thermochim. Acta 190 (1991) 143.
[10] M. Maciejewski, H.R. Osward, Thermochim. Acta 85 (1985) 39.
[11] M. Maciejewski, J. Baldyaga, Thermochim. Acta 92 (1985) 105.
[12] Romeo Salvador, E. Gracia Calvo, C. Beneitez Aparicio, Thermochim. Acta 143 (1989) 339.

[13] J.M. Criado, A. Ortega, Thermochim. Acta 195 (1992) 163.
[14] K.J.D. Mackenzie, N. Hadipour, Thermochim. Acta 35 (1980) 227.
[15] D. Price, N. Fatemi, D. Dollimore, R. Whitehead, Thermochim. Acta 94 (1985) 313.
[16] N.D. Topor, L.I. Tolokonnikova, B.M. Kadenatsi, J. Thermal. Anal. 22 (1981) 221.
[17] J. Peric, R. Kristulovic, J. Ferie, M. Vacak, Thermochim. Acta 207 (1992) 245.
[18] J. Morales, L. Herman, L.V. Flores, A. Ortega, J. Thermal. Anal. 24 (1982) 23.
[19] J.B. Dubrawski, B.M. England, J. Thermal. Anal. 39 (1993) 987.
[20] M. Epple, J. Thermal. Anal. 45 (1995) 1265.
[21] A.W. Searcy, D. Beruto, J. Phys. Chem. 804 (1976) 425.
[22] M. Kamruddin, P.K. Ajikumar, S. Dash, B. Purniah, A.K. Tyagi, K. Krishan, Instrument. Sci. Technol. 233 (1995) 123.
[23] S. Dash, M. Kamruddin, A.K. Tyagi, Bull. Mater. Sci. 20 (3) (1997) 359.
[24] J.M. Criado, M. Gonzalez, J. Malek, A. Ortega, Thermochim. Acta 254 (1995) 121.
[25] P.D. Garn, Thermoanalytical Methods of Investigation, Academic Press, New York, 1965, p. 247.
[26] Marek Maciejewski, Armin Reller, Thermochim. Acta 110 (1987) 145.
[27] J.M. Thomas, G.D. Renshaw, Chem. Commun. 1247 (1968).
[28] D. Beruto, A.W. Searcy, J. Chem. Soc., Faraday Trans. I 70 (1974) 2145.
[29] T.C.W. Mak, Gong Du. Zhou, Crystallography in Modern Chemistry, Wiley, New York, 1992, p. 146.
[30] H. Chessin, W.C. Hamilton, Acta Cryst. 18 (1965) 689.
[31] L.E. Reichl, A Modern Course in Statistical Physics, University of Texas, Austin, 1980, p. 107.
[32] A. Kotter (Ed.), Structure and Properties of Ceramics, Elsevier, Amsterdam, 1994, p. 65.
[33] H. Mc Murdaie, Powder Diffraction 1 (1986) 266.
[34] B.K. Vainshitein, Modern Crystallography I, Springer, Berlin, 1981, p.314.
[35] R.S. Krishnan, R. Srinivasan, S. Devanarayanan, Thermal Expansion of Crystals, Pergamon Press, Oxford, 1979.
[36] L.D. Landau, E.M. Lifshitz, in: E.M. Lifshitz, L.P. Pitaevskii (Eds.), Statistical Physics, 3rd Edition (RUN), Vol. 5, Part I, Pergamon Press, Oxford, 1980, p. 195.
[37] R. Ruppin, Solid State Commun. 10 (1972) 1053.
[38] D. Beruto, A.W. Searcy, Nature 263 (1976) 221.
[39] K.M. Towe, Nature 274 (1978) 239.
[40] J.M. Thomas, G.D. Renshaw, J. Chem. Soc. A (1967) 2058.
[41] S. Surinach, J. Malagelada, M.D. Baro, in: A.R. Javeri (Ed.), Metastable, Mechanically Alloyed, Nanocrystalline Materials, Transtech Publication, 1995, p. 357.
[42] K. Binder, in: R.W. Cahn, P. Haasen, E.J. Kramer (Eds.), Materials Science and Technology, Vol. 5, P. Haasen (Ed.), Phase Transformation in Materials, VCH, Weinheim, 1991, p. 202.
[43] V.S. Raghunathan, S. Raju, A.L.E. Terrance, in: D. Banerjee, L.A. Jocobson (Eds.), Metastable Microstructure, Oxford and ZBH Publishing Co., New Delhi, 1993, p. 161.
[44] R. Morell, in: R.W. Cahn, P. Haasen, E.J. Kramer (Eds.), Materials Science and Technology, 17 A, R.J. Brook (Ed.), Processing of Ceramics, Vol. I, VCH, Weinheim, p. 12.
[45] W.R. Moser, J.E. Sunstrom, B. Marshik-Guerts, W.R. Moser (Eds.), Advanced Catalysts and Nanostructured Materials, Academic Press, San Diego, 1996, p. 285.